Inorganic Chemistry

ARTICLE

pubs.acs.org/IC

# Thermochromic Luminescence of Copper Iodide Clusters: The Case of Phosphine Ligands

Sandrine Perruchas,*[,†] Cédric Tard,[†] Xavier F. Le Goff,[‡] Alexandre Fargues,[§] Alain Garcia,[§] Samia Kahlal,[⊥,∥] Jean-Yves Saillard,[⊥,∥] Thierry Gacoin,[†] and Jean-Pierre Boilot*[,†]

[†]Laboratoire de Physique de la Matière Condensée (PMC) and [‡]Laboratoire Hétéroéléments et Coordination (DCPH), CNRS−Ecole Polytechnique, 91128 Palaiseau Cedex, France

[§]Institut de Chimie de la Matière Condensée de Bordeaux (ICMCB)−CNRS, 87 Avenue du Docteur A. Schweitzer, 33608 Pessac Cedex, France

[⊥]UMR-CNRS, 6226 "Sciences Chimiques de Rennes", Université de Rennes 1, 35042 Rennes Cedex, France

[∥]Université Européenne de Bretagne, 5 bd. Laënnec, 35000 Rennes, France

Supporting Information

**ABSTRACT:** Three copper(I) iodide clusters coordinated by different phosphine ligands formulated $[Cu_4I_4(PPh_3)_4]$ (**1**), $[Cu_4I_4(Pcpent_3)_4]$ (**2**), and $[Cu_4I_4(PPh_2Pr)_4]$ (**3**) ($PPh_3$ = triphenylphosphine, $Pcpent_3$ = tricyclopentylphosphine, and $PPh_2Pr$ = diphenylpropylphosphine) have been synthesized and characterized by $^1H$ and $^{31}P$ NMR, elemental analysis and single crystal X-ray diffraction analysis. They crystallize in different space groups, namely, monoclinic $P21/c$, cubic $Pa\bar{3}$, and tetragonal $I\bar{4}2m$ for **1**, **2**, and **3**, respectively. The photoluminescence properties of clusters **1** and **3** show reversible luminescence thermochromism with two highly intense emission bands whose intensities are temperature dependent. In accordance to Density Functional Theory (DFT) calculations, these two emission bands have been attributed to two different transitions, a cluster centered (CC) one and a mixed XMCT/XLCT one. Cluster **2** does not exhibit luminescence variation in temperature because of the lack of the latter transition. The absorption spectra of the three clusters have been also rationalized by time dependent DFT (TDDFT) calculations. A simplified model is suggested to represent the luminescence thermochromism attributed to the two different excited states in thermal equilibrium. In contrast with the pyridine derivatives, similar excitation profiles and low activation energy for these phosphine-based clusters reflect high coupling of the two emissive states. The effect of the Cu−Cu interactions on the emission properties of these clusters is also discussed. Especially, cluster **3** with long Cu−Cu contacts exhibits a controlled thermochromic luminescence which is to our knowledge, unknown for this family of copper iodide clusters. These phosphine-based clusters appear particularly interesting for the synthesis of original emissive materials.

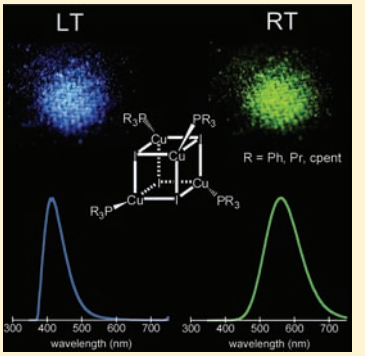


## INTRODUCTION

Research on luminescent compounds has been actively pursued in the past two decades because of their numerous potential applications in light emitting devices.[1,2] The $d^{10}$ coinage metal compounds are known to present a great variety of structural forms associated with rich photophysical properties.[3−5] Among them, the tetracopper(I) clusters formulated $[Cu_4X_4L_4]$ (X = Cl, Br, I; L = pyridine or amine-based derivatives) are an interesting family of polynuclear complexes which present original and remarkable luminescence behavior.[4,6] The molecular structure of these cubane type clusters is represented in Figure 1 with copper and halide atoms occupying alternatively the corner of a cube.

In this family of compounds, the iodide cluster derivatives are known to exhibit higher luminescence quantum yield and stability compared to the chloride and bromide analogues.[4] The iodide cluster coordinated by pyridine, namely, $[Cu_4I_4py_4]$, has been the most intensively studied member of this family. This cluster is highly luminescent at room temperature, and this emission is strikingly sensitive to the temperature and the environment such as the rigidity of the host medium. The thermochromic luminescence[7] observed originates from two emission bands of different energy whose relative intensities vary in temperature.[8] At room temperature, the luminescence is dominated by a low energy band (LE) which has been attributed, on the basis of experimental data[4] and Density Functional Theory (DFT) calculations,[9] to a combination of a halide-to-metal charge transfer (XMCT) and copper-centered $d \rightarrow s, p$ transitions. This emission is called "cluster centered" (CC) as it involves a $[Cu_4I_4]$ cluster centered triplet excited state. At low temperature, this band is extremely weak, and the emission is dominated by a higher energy band (HE) which has been attributed to a triplet halide-to-pyridine charge-transfer (XLCT) excited state. On the basis of previous studies on copper halide complexes, the

**Received:** May 26, 2011
**Published:** September 29, 2011





dx.doi.org/10.1021/ic201128a | *Inorg. Chem.* 2011, 50, 10682–10692

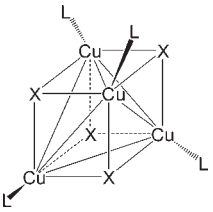


**Figure 1.** General representation of $[Cu^{I}_4X_4L_4]$ clusters (X = Cl, Br, I; L = organic ligand).

**Chart 1. Designation of the Clusters Studied**

| | |
|---|---|
| $[Cu_4I_4(PPh_3)_4]$ | **1** |
| $[Cu_4I_4(Pcpent_3)_4]$ | **2** |
| $[Cu_4I_4(PPh_2Pr)_4]$ | **3** |

thermochromic luminescence property appears to be specific to the $[Cu_4X_4L_4]$ cubane molecular form of the clusters.[4,10,11]

These emissive properties make these copper clusters particularly attractive to synthesize materials with original optical applications. With this purpose, we have reported the study of silica sol−gel films incorporating $[Cu_4I_4L_4]$ clusters coordinated by phosphine ligands.[12] For the first time, the thermochromic luminescence behavior was observed for clusters bearing phosphine ligands, and preliminary analysis shows some interesting difference with the pyridine derivatives. Actually, compared to the latter, only scarce photophysical studies of $[Cu_4X_4L_4]$ clusters with L = phosphine ligands are available in the literature. The synthesis and structural characterizations of several $[Cu_4I_4L_4]$ clusters have been, however, described in the literature. Ligands involved are $PEt_3$,[13] $P(NMe_2)_3$,[14] $PPh_2Me$,[15] $PPh_3$,[16] dmpp (1-phenyl-3,4-dimethylphosphole),[17] $PPh_2Fc$ (Fc = ferrocene derivatives),[18] $P^tBu_3$,[19] $P(chept)_3$ (chept = cyclohepta-2,4,6-trienyl),[20] $P(pTol)_3$ (Tol = *p*-tolyl),[21] $PPh_2(CyHexyl)$,[22] $P(ddppd)_3$[23] (ddppd = $\mu_2$-3,8-dioxo-1,10-bis(diphenylphosphino)-4,7-diazadecane-P,P′) and $PPh_2(CH_2CH{=}CH_2)$.[24] Among this series, the luminescence studies reported have only concerned the clusters formulated $[Cu_4I_4L_4]$ (L = dmpp, $P^nBu_3$, $PPh_3$, and $PPh_2(CH_2CH{=}CH_2)$).[25,4,26,24] The emission observed for the latter three has been attributed, in analogy with the $[Cu_4I_4py_4]$ cluster, to the LE (XMCT/d → s, p) and HE (XLCT) bands previously cited. For $[Cu_4I_4(dmpp)_4]$, the emission was assigned to a metal-to-ligand charge-transfer transition (MLCT) based on vibronic structure analyses. From these studies, the emissions observed seem to have different origin, and no theoretical study has been realized to clearly established the nature of the molecular states involved. To better comprehend the photophysical properties of these copper iodide clusters and definitively establish the origin of the electronic transitions, we have investigated, both experimentally and theoretically, several phosphine-based cooper iodide clusters.

Herein, we report on the synthesis, structural characterizations, optical properties, and theoretical study of $[Cu_4I_4L_4]$ clusters with phosphine ligands. Three clusters (Chart 1) have been studied which are coordinated with different phosphine ligands: triphenylphosphine ($PPh_3$), tricyclopentylphosphine ($Pcpent_3$), and diphenylpropylphosphine ($PPh_2Pr$) which are represented in Figure 2. Light emission properties of the clusters have been studied in detail as a function of the temperature (from

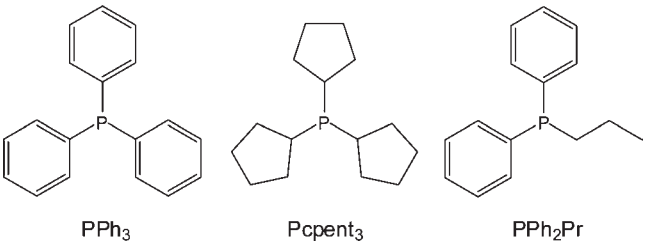


**Figure 2.** Phosphine ligands studied.

290 to 8 K) showing reversible luminescence thermochromism with two highly intense emission bands for two of these clusters. To rationalize the photophysical properties observed, DFT calculations have been performed for the three clusters as well as for the model cluster $[Cu_4I_4(PH_3)_4]$. This study gives straightforward explanation for the different luminescence behavior observed for clusters **1** and **3**, and cluster **2**. The geometry of the singlet ground state ($S_0$) and of the two lowest triplet states ($T_1$ and $T_2$) of the clusters has been optimized. The nature of the excited state involved in the absorption spectrum and those responsible of the two different emission bands observed for these clusters have been characterized using time dependent DFT (TDDFT) calculations. In analogy with previous studies on copper iodide clusters with pyridine derivatives, a simplified energy diagram is suggested illustrating the luminescence thermochromism observed.

## EXPERIMENTAL SECTION

**Synthesis.** All manipulations were performed with standard air-free techniques using Schlenk equipment, unless otherwise noted. Solvents were distilled from appropriate drying agents and degassed prior to use. Copper(I) Iodide, triphenylphosphine, and tricyclopentylphosphine were purchased from Aldrich and used as received. Synthesis of **1** has been adapted from ref 16 and that of **3** has been already reported.[12]

***Caution!*** *Tricyclopentylphosphine is a pyrophoric compound, handling with care is recommended.*

**1.** To a suspension of CuI (500 mg, 2.6 mmol) in toluene (50 mL) was added triphenylphosphine (700 mg, 2.6 mmol). The solution was stirred for 12 h at 110 °C. The solution was filtrated and after cooling down to room temperature the product was recovered as colorless bulk crystals. Yield = 61% (0.72 g, 0.4 mmol). $^1$H NMR (300 MHz, $CD_2Cl_2$): $\delta$ (ppm) 7.57−7.31 (m, $C_6H_5$); $^{31}$P NMR (300 MHz, $CD_2Cl_2$): $\delta$ (ppm) −21.0 (br). Anal. Calcd for $C_{72}H_{60}P_4Cu_4I_4$: C, 47.73; H, 3.31. Found: C, 47.84; H, 3.32.

**2.** To a suspension of CuI (1.25 g, 6.6 mmol) in dichloromethane (20 mL) was added tricyclopentylphosphine (1 g, 4.2 mmol). The solution was stirred for 12 h at room temperature. The mixture was filtrated, and after slow addition of ethanol the product was recovered as colorless crystals. Yield = 67% (1.2 g, 0.7 mmol). $^1$H NMR (300 MHz, $CDCl_3$): $\delta$ (ppm) 2.13−1.51 (m, $C_5H_9$); $^{31}$P NMR (300 MHz, $CDCl_3$): $\delta$ (ppm) −2.61 (br). Anal. Calcd for $C_{60}H_{108}P_4Cu_4I_4$: C, 42.00; H, 6.30. Found: C, 41.97; H, 6.32.

**Characterizations.** $^1$H and $^{31}$P liquid NMR spectra were recorded on an Bruker AvanceII300 spectrometer at room temperature, operating at the radiofrequency of 300 MHz. $^1$H spectra were internally referenced from peaks of residual protons in deuterated solvents or from tetramethylsilane (TMS). A solution of $H_3PO_4$ 85% weight was used as an external standard for $^{31}$P spectra. Elemental analyses (C, H) were performed by the Service Central d'Analyses−CNRS of Vernaison.

Luminescence spectra were recorded on a SPEX Fluorolog FL 212 spectrofluorimeter (Horiba Jobin Yvon). The excitation source is a

450 W xenon lamp, and excitation spectra were corrected for the variation of the incident lamp flux, as well as emission spectra for the transmission of the monochromator and the response of the photomultiplier (Peltier cooled Hamamatsu R928P photomultiplier). Low temperature measurements have been done with a liquid helium circulation cryostat SMC TBT Air Liquid model C102084.

The internal (absolute) quantum luminescence yields ($Q_{int}$) of the clusters have been determined according to the following equation $Q_{int} = Q_{ext}/(Abs)$. The external quantum yields ($Q_{ext}$) were obtained by comparison with the calibrated reference powder sample ($Zn_2SiO_4$: Mn National Bureau of Standard NBS 1028: $Q_{ext.\lambda ex260\ nm} = 0.70$)[27] (Supporting Information, Figure S2). The absorption distributions (Abs) were measured from a diffuse reflectance experiment using the synchronous scan technique: excitation and emission monochromators were moved simultaneously at the same wavelength with a defocalized sample position and with the collected light in a fixed Ω solid angle. The absorption distributions were corrected with two reference compounds, MgO and carbon-black. Note that the validity of our method has been previously checked with the use of an integrating sphere apparatus.

Emission lifetimes were recorded with an Edinburg spectrofluorimeter equipped with a nanoflash $H_2$ lamp (0.37 bar) using the TCSPC (Time Correlated Single Photon Counting) method. Data were analyzed by exponential curve fitting and are reported in Supporting Information, Figure S8.

UV−visible absorption spectra were recorded with a Varian Cary 50 spectrophotometer with dichloromethane solutions of the clusters ($c = 1.2 \times 10^{-4}$ mol $L^{-1}$).

**X-ray Structure Determination.** Single crystals suitable for X-ray structure determination were obtained for clusters **1**−**2** as described in the synthesis section. Crystals were mounted on fiberglass using paraton oil and immediately cooled to 150 K in a cold stream of nitrogen. All data were collected on a Nonius Kappa CCD diffractometer at 150(1) K using a Mo $K_\alpha$ ($\lambda$ = 0.71073 Å) X-ray source and a graphite monochromator. The cell parameters were initially determined using more than 50 reflections. Experimental details are described in Supporting Information, Table S1. The crystal structures were solved in SIR 97[28] and refined in SHELXL-97[29] by full-matrix least-squares using anisotropic thermal displacement parameters for all non-hydrogen atoms. All the hydrogen atoms were placed in geometrically calculated positions. Details of crystal data and structure refinements are summarized in the Supporting Information, Table S1.

**Computational Details.** DFT calculations have been carried out with the program Gaussian03,[30] using the PBE1PBE (PBE0)[31] functional and a standard double-$\xi$ polarized basis set, namely, the LANL2DZ set,[32] augmented with polarization functions on all atoms, that is, a p orbital with exponent 0.8 for H, a d orbital with exponents 0.8, 0.55, and 0.309 for C, P, and I, respectively, and an f orbital with exponent 0.8 on Cu. Spin-unrestricted calculations were performed in the case of triplet states. Geometry optimizations of the ground states of clusters **1**−**3** have been carried out starting with their experimental X-ray geometries, slightly idealized in the case of **1** and **3**. In these two latter cases, the optimized idealized structure was found almost identical as the one obtained by starting with the less symmetrical experimental one. Because of Jahn−Teller effect, the triplet states were found to adopt lower symmetries. Vibrational frequencies have been calculated on all the optimized structures. Only in the case of **3**, non negligible imaginary frequencies were computed ($\sim$ 100i $cm^{-1}$). Any attempt to lower the symmetry in following the displacements associated with these imaginary frequencies resulted in serious convergence problems during optimization. Since these displacements were found to involve exclusively the propyl groups, it was decided to disregard these small imaginary frequencies in the following analyses which concern properties specifically associated with the $[Cu_4I_4]$ cluster core. The composition of the molecular orbitals was calculated using the AOMix program.[33] The UV visible transitions were calculated by means of time dependent DFT (TDDFT) calculations[34] at the same level of theory. The 120, 50, 80, and 80 singlet−singlet transitions of lowest energy have been computed for $[Cu_4I_4(PH_3)_4]$, **1**, **2**, and **3**, respectively. This corresponds to wavelengths larger than 194, 269, 204, and 248 nm for $[Cu_4I_4(PH_3)_4]$, **1**, **2**, and **3**, respectively. Only transitions with oscillator strengths larger or equal to 0.01 are reported and discussed. Representation of the molecular structures has been done using the program MOLEKEL 4.3.[35]

## RESULTS

**Synthesis and Structural Characterization of the Clusters.** Clusters **1**−**3** were synthesized in solution from CuI and the corresponding phosphine ligands. All clusters were obtained as colorless crystals (see Experimental Section). They were characterized by elemental analyses and by $^1H$ and $^{31}P$ liquid NMR. Crystal structures of clusters **1**−**2** were solved by single crystal X-ray diffraction analysis at 150 K and the data of **3**, already published,[12] are reported for discussion and comparison. Note that the crystal structure of **1** has been already reported in the literature[16,26] but for the sake of comparing data (same experimental conditions especially the temperature), here are reported our data. The three clusters crystallize in different space groups, monoclinic $P21/c$, tetragonal $I\bar{4}2m$, and cubic $Pa\bar{3}$ for **1**, **3**, and **2**, respectively. The unit cell contents are shown in Supporting Information, Figure S1. All three structures can be described as an assembly of columns of clusters. For **1**, the columns run along the *a* axis and the cluster orientation changes alternatively from one column to the other. For **2**, the cluster columns run also along the *a* axis, but in this case in a single column the clusters are alternatively shifted along the *c* axis. For **3**, the columns of clusters are along the *c* axis and are all identical.

The molecular structures of the clusters are depicted in Figure 3. The three clusters present a cubane structure formed by four copper atoms and four iodine atoms which occupy alternatively the corners of a distorted cube. Actually, the $[Cu_4I_4]$ core can also be described as a copper tetrahedron embedded within a larger iodine tetrahedron. The phosphine ligands are coordinated to each copper atom by the phosphorus atom. Cluster **2** is located on a 3 axis corresponding to the larger diagonal of the $[Cu_4I_4]$ cubane core. Cluster **3** possesses a $\bar{4}$ axis which crosses the middle of a $[Cu_2I_2]$ face. Cluster **1** has no particular position. Formulations for the **1**−**3** clusters are in agreement with NMR and elemental analysis.

Selected bond lengths and angles of the clusters are listed in Supporting Information, Table S2, and mean values are reported in the caption of Figure 3. The ligands present a classical geometry for phosphine derivatives. The Cu−P values are similar for clusters **1** (2.255(1) Å) and **3** (2.25(2) Å) and are comparable with other copper iodide clusters coordinated with phosphine derivatives.[13−23] However, in cluster **2** the Cu−P bonds are significantly shorter (2.234(2) Å). Short Cu−P bonds are also found in cluster $[Cu_4I_4(P(NMe_2)_3)_4]$ (mean 2.231 Å).[14] This effect can be attributed to steric hindrance of the groups bonded to the phosphorus atoms. The Cu−I bond distances for the three clusters are similar and within the range of reported values for this type of clusters with phosphine ligands. The I−Cu−I angle mean values for all the clusters are comparable, but for cluster **1** and **3** these values present a larger range (103.44(1)−115.59(2)° and 100(2)−108(1)° respectively) compared with cluster **2** (102.64 (2)−104.93(2)°). The latter has thus a less distorted $[Cu_4I_4]$

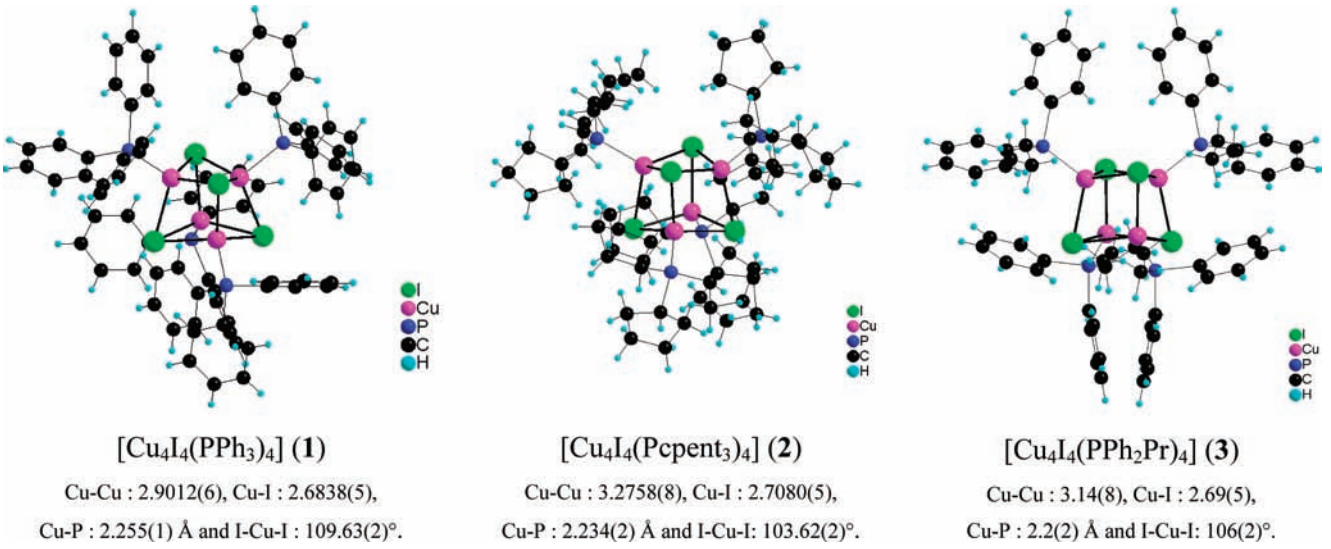


**Figure 3.** Molecular structure of clusters **1**−**3** and mean of selected bond lengths.

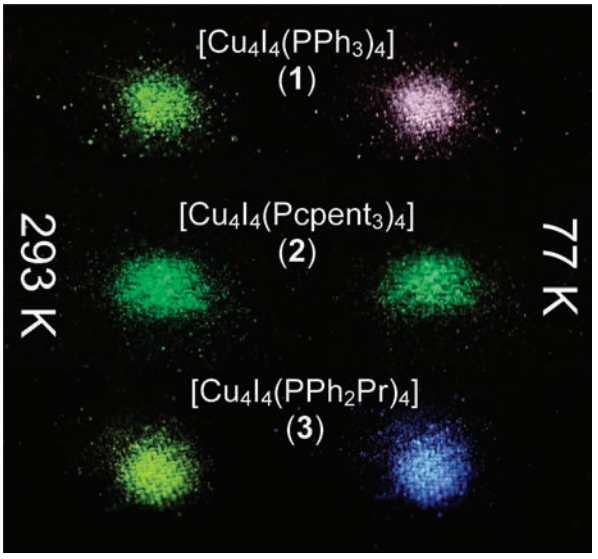


**Figure 4.** Photos of powder of clusters **1**−**3** under UV irradiation at 312 nm (UV lamp) at room temperature (left) and in liquid nitrogen (right).

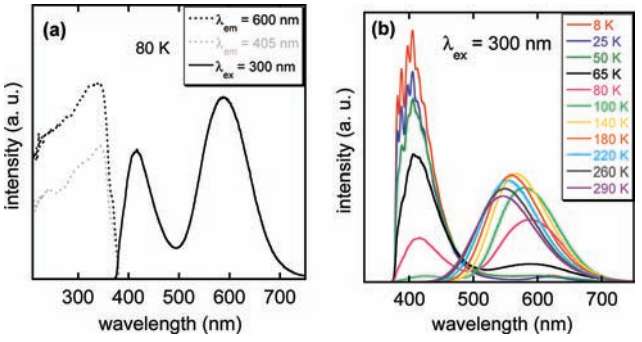


**Figure 5.** Temperature dependence of solid-state luminescence spectra of **1**; (a) emission (solid lines) at 80 K with corresponding excitation spectra (dotted lines) and (b) emission spectra from 290 to 8 K with $\lambda_{ex}$ = 300 nm.

cube. Cluster **1** presents the shortest Cu−Cu bond lengths with an average distance of 2.901(1) Å. The values for clusters **2** and **3**, 3.276(1) and 3.14(8) Å, respectively, are slightly longer than those found in the literature for similar clusters with phosphine bearing phenyl derivatives: $[Cu_4I_4(PPh_2CH_3)_4]$[15] (mean 2.930 Å, range 2.840−3.010 Å at 295 K), $[Cu_4I_4(PPh_2CyHexyl)_4]$[22] (mean 2.951 Å, range 2.863−3.057 Å at 100 K), and $[Cu_4I_4(pTol)_4]$[21] (mean 3.023 Å, range 2.975−3.071 Å at 193 K). Note that even longer Cu−Cu contacts are found for clusters $[Cu_4I_4(Pchept_3)_4]$[20] (mean 3.247, range 3.061−3.382 Å at 293 K), $[Cu_4I_4(P(NMe_2)_3)_4]$[14] (mean 3.386 range 3.283−3.465 Å at 295 K), and $[Cu_4I_4(P^tBu_3)_4]$ (mean 3.560 range 3.551−3.559 Å at 100 K).[19] Accordingly to previous studies, the Cu−Cu bonds in $[Cu_4I_4L_4]$ clusters based on phosphine ligands are significantly longer compared with those found in pyridine or amine derivatives.[36] For example, in $[Cu_4I_4py_4]$, the Cu−Cu bond distances are in the range 2.619−2.721 Å with a mean value of 2.690 Å.[37] This value is shorter than the sum of the van der Waals radii of copper(I) (2.80 Å),[38] and thus imply strong metal−metal bonding interactions in this cluster. For clusters **2** and **3** it is obvious that no or weak Cu−Cu interactions exist but for cluster **1** the question is open. This point is important since Cu−Cu interactions have been reported to greatly influence the luminescence properties of these copper iodide clusters. This is discussed further in the following part.

**Optical Properties.** Clusters **1**−**3** are white powders under ambient light. At room temperature, under UV irradiation, these clusters emit an intense green light as shown in Figure 4. The thermochromic luminescence of clusters **1** and **3** is revealed by dipping the samples into liquid nitrogen. Under the same UV excitation, the green emission is replaced by a purple or a blue one whereas the emission of cluster **2** is still green (Figure 4). When the sample is progressively warmed up to room temperature, the green emission is recovered, indicating a completely reversible thermochromic luminescence for clusters **1** and **3**.

Solid-state emission and excitation spectra have been recorded for clusters **1**−**3** from room temperature down to 8 K

**Table 1. Photoluminescence Data at Different Temperatures of Clusters 1−3**

| compound | $T$ (K) | $\lambda^{max}_{em}$ (nm) [$\lambda_{ex}$ (nm)] | band attribution |
|---|---|---|---|
| $[Cu_4I_4(PPh_3)_4]$ (**1**) | 290 | 545 [300] | LE |
| | 120 | 570 [300] | LE |
| | 80 | 587 [300] | LE |
| | | 415 [300] | HE |
| | 8 | 405 [300] | HE |
| $[Cu_4I_4(Pcpent_3)_4]$ (**2**) | 290 | 523 [290] | LE |
| | 80 | 515 [290] | LE |
| | 8 | 515 [290] | LE |
| $[Cu_4I_4(PPh_2Pr)_4]$ (**3**) | 290 | 560 [330] | LE |
| | 100 | 566 [330] | LE |
| | | 424 [330] | HE |
| | 8 | 412 [330] | HE |

(Figures 5−7) and corresponding data are reported Table 1. Note that preliminary emission data of cluster **1** and **3** have been already reported,[12,26] but here, their photophysical properties are studied in the same experimental conditions as **2**, especially luminescence is reported at lower temperature down to 8 K. At 290 K, the emission spectra display a single unstructured broad emission band centered at 545 nm ($\lambda_{ex}$ = 300 nm) for **1**, at 523 nm ($\lambda_{ex}$ = 290 nm) for **2**, and at 560 nm ($\lambda_{ex}$ = 330 nm) for **3** in agreement with the yellow-green light observed at room temperature. The internal quantum yields of the clusters have been determined at room temperature (see Experimental Section), and the high values obtained exciting at 260 nm are 64, 23, and 60% for **1**, **2**, and **3**, respectively.

By lowering the temperature, a new emission band (HE) appears at higher energy for clusters **1** and **3** (Figures 5 and 7 respectively). This new band progressively increases in intensity with the concomitant extinction of the green band (LE). At 80 K, the two emission bands are present with maxima at 415 and 587 nm for **1** and at 424 and 566 nm for **3** at 100 K. The addition of the green and the blue lights gives the purple emission observed for cluster **1** in liquid nitrogen. For cluster **3**, the contribution of the blue band is higher so the emission observed is bluer (Figure 4). At 8 K, only the blue band is observed at 405 nm for **1** and at 412 nm for **3**. In both cases, the excitation profiles of the two emission bands are similar with maxima at 330 nm for **3** and at 340 nm for **1** (Figure 5−7a). The Stokes shift between excitation and emission maxima of the LE band, 12380 and 12635 $cm^{-1}$ for clusters **1** (at 80 K) and **3** (at 100 K) respectively, are thus much larger compared to those of the HE band 5320 and 6720 $cm^{-1}$. A striking feature of the blue band of **1** is the vibronic structure observed at low temperature (Figure 5b). The luminescent behavior of cluster **2** contrasts with that of **1** and **3**. Indeed, as shown Figure 6, despite narrowing of the bandwidth, the green emission position is almost unchanged by lowering the temperature with maxima at 523 nm at 290 K and at 515 nm at 8 K ($\lambda_{ex}$ = 290 nm). The excitation profile of the emission band is also in this case, similar whatever the temperature with maximum at 295 nm (Figure 6a). The Stokes shift between excitation and emission maxima is 14410 $cm^{-1}$ at 290 K.

Temperature dependent luminescence spectra between 292 and 8 K are shown in Figure 5−7b. For cluster **1**, a red shift is clearly observed for the LE emission band by decreasing the temperature. For example, at 290 K the maximum emission is at

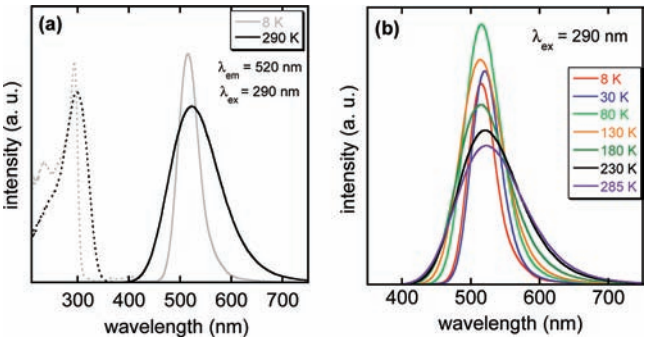


**Figure 6.** Temperature dependence of solid-state luminescence spectra of **2**; (a) emission (solid lines) at 290 and 8 K with corresponding excitation spectra (dotted lines) and (b) emission spectra from 285 to 8 K with $\lambda_{ex}$ = 290 nm.

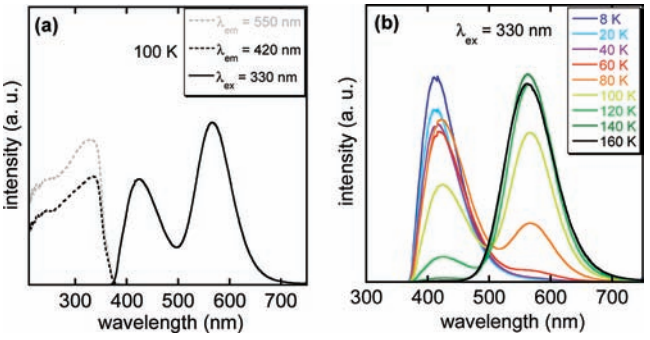


**Figure 7.** Temperature dependence of solid-state luminescence spectra of **3**; (a) emission (solid lines) at 100 K with corresponding excitation spectra (dotted lines) and (b) emission spectra from 160 to 8 K with $\lambda_{ex}$ = 330 nm.

$\lambda_{max}$ =545 nm whereas at 120 K it is at 570 nm. In contrast, no shift is observed for clusters **2** and **3**; the position of the LE band does not vary significantly with the temperature. As already mentioned, for all clusters, excitation spectra recorded between 8 and 290 K do not show any significant difference (figures in Supporting Information).

For cluster **3**, in the 8−160 K range, all the emission curves seem to cross at one point, in particular the 80−120 K curves present an isoemissive point at 500 nm. This is characteristic of two states in thermal equilibrium, which are in our case the emission from the two LE and HE excited states. After integration of the peaks, an Arrhenius plot leads to an activation energy value of $E_a$ = 5784 J (483 $cm^{-1}$), corresponding to the energy barrier between the two emission states in thermal equilibrium (Supporting Information, Figure S6).

Emission lifetimes have been determined for the cluster $[Cu_4I_4(PPh_3)_4]$ (**1**), and the corresponding spectra are reported in Supporting Information, Figure S8. At 290 K, the LE emission band lifetime value is 4.3 $\mu$s. At 77 K, where the two emissions are present, the lifetime value recorded for the HE band is 14.2 $\mu$s. Whereas those data present single exponential decays, the data recorded for the LE band at 77 K presents a different feature with first a rising time ($\tau$1 = 6.4 $\mu$s) followed by a classical decay ($\tau$2 = 15.4 $\mu$s).

**Electronic Structure of the Ground and Excited States.** To rationalize the optical properties observed, DFT calculations

Table 2. Relevant Computed Data for $[Cu_4I_4(PH_3)_4]$, 1, 2, and 3[a]

| | $[Cu_4I_4(PH_3)_4]$ | | $[Cu_4I_4(PPh_3)_4]$ (1) | | | $[Cu_4I_4(Pcpent_3)_4]$ (2) | | | $[Cu_4I_4(PPh_2Pr)_4]$ (3) | | |
|---|---|---|---|---|---|---|---|---|---|---|---|
| | $S_0$ ($T_d$) | $T_1$ ($C_{3v}$) | $S_0$ ($T$) | $T_1$ ($C_2$) | $T_2$ ($C_1$) | $S_0$ ($C_3$) | $T_1$ ($C_1$) | $T_2$ ($C_1$) | $S_0$ ($D_{2d}$) | $T_1$ ($C_{2v}$) | $T_2$ ($C_s$) |
| relative energy (eV) | 0.00 | 3.30 | 0.00 | 3.29 | 3.38 | 0.00 | 3.32 | | 0.00 | 3.54 | 3.12 |
| Cu−Cu (Å) range | 2.833 | 2.570−2.582 | 3.040−3.040 [2.776−3.100] | 2.576−2.666 | 2.941−3.035 | 3.146−3.242 [3.265−3.286] | 2.635−2.756 | | 3.220−3.388 [3.08−3.26] | 2.575−2.747 | 3.094−3.283 |
| mean | | 2.576 | 3.040 [2.901] | 2.635 | 3.016 | 3.194 [3.276] | 2.678 | | 3.276 [3.14] | 2.702 | 3.154 |
| Cu−I (Å) range | 2.738 | 2.763−3.066 | 2.740 [2.650−2.712] | 2.806−3.145 | 2.680−2.760 | 2.741−2.781 [2.686−2.755] | 2.741−3.091 | | 2.752−2.853 [2.67−2.70] | 2.800−3.292 | 2.707−2.783 |
| mean | | 2.943 | 2.740 [2.684] | 2.916 | 2.725 | 2.736 [2.708] | 2.927 | | 2.786 [2.69] | 2.928 | 2.735 |
| Cu−P (Å) range | 2.346 | 2.291−2.315 | 2.357 [2.258−2.253] | 2.368−2.380 | 2.34−2.37 | 2.341−2.344 [2.233−2.234] | 2.381−2.446 | | 2.360 [2.2 ] | 2.417−2.433 | 2.376−2.396 |
| mean | | 2.309 | 2.357 [2.255] | 2.374 | 2.355 | 2.342 [2.234] | 2.399 | | | 2.425 | 2.386 |
| Cu−I−Cu (deg) mean | 62 | 52 | 67 [65] | 54 | 67 | 71 [75] | 55 | | 73 [71] | 55 | 70 |

[a] Values in brackets are X-ray experimental data.

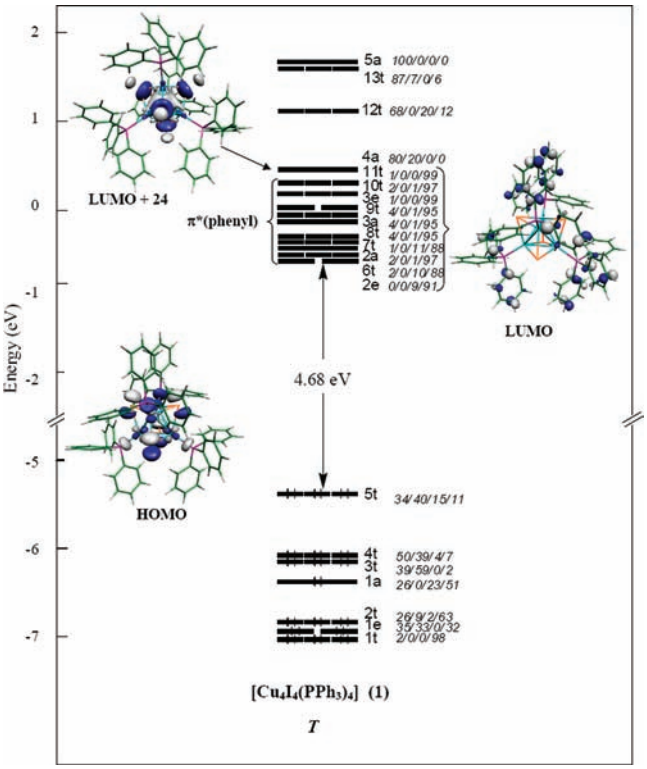


**Figure 8.** MO diagram of **1**. The localization of each MO is given (in %) in the following order: Cu/I/P/phenyl.

have been performed on clusters **1**−**3**, as well as on the model cluster $[Cu_4I_4(PH_3)_4]$. The geometries of the singlet ground state ($S_0$) and of the lowest triplet state ($T_1$) have been optimized for the four compounds. The second lowest triplet state ($T_2$) was also investigated in the case of compounds **1** and **3** (see below). Relevant data computed for all these states are provided in Table 2, and the experimental (X-ray) metrical data are reported in brakets beside the corresponding ground-state $S_0$ values. These values are in fair agreement with a slight general overestimation of the computed distances compared to the experimental ones.

The electronic structures of the ground states of the four clusters have been investigated. The molecular orbital diagram of $[Cu_4I_4(PPh_3)_4]$ (**1**) is represented in Figure 8, whereas the three other ones are provided in Supporting Information, Figure S7). The nine highest occupied molecular orbitals (HOMOs) of **1** are mainly composed of 3d(Cu) and 5p(I) orbitals. In particular, the triply degenerate 5t HOMO is made of similar contributions of Cu (34%) and of I (40%). The closely spaced 24 lowest unoccupied molecular orbitals (LUMOs) are largely dominated by their phosphine character (88−99%). They correspond to the combinations of the $\pi^*$ orbitals of the phenyl groups (two $\pi^*$ orbitals per phenyl group). Lying just above this block of 24 MOs, the 4a level is dominated by its 4s/4p(Cu) character (80%), with some iodine admixture (20%). This orbital is significantly Cu−Cu bonding with some Cu−I antibonding character. Its energy is very sensitive to the Cu−Cu distances: the shortest the Cu−Cu distances, the lowest the energy of this orbital is. The existence of such a vacant bonding combination of a 4s/4p(Cu) hybrid of $a_1$ (or a) symmetry agrees with previous calculations on $[Cu_4X_4L_4]$ (X = H, $CH_3$, CCH, F, Cl, Br, I;

**Table 3. Optical Calculated and Experimental Data for $[Cu_4I_4(PH_3)_4]$ and 1−3**[a]

| | compound | | | | | | |
|---|---|---|---|---|---|---|---|
| | $[Cu_4I_4(PH_3)_4]$ | $[Cu_4I_4(PPh_3)_4]$ (**1**) | | $[Cu_4I_4(Pcpent_3)_4]$ (**2**) | | $[Cu_4I_4(PPh_2Pr)_4]$ (**3**) | |
| data | calc. | exp. | calc. | exp. | calc. | exp. | calc. |
| absorption $\lambda$ nm ($f \geq 0.01$) | **243** (0.11)<br>$4t_2 \rightarrow 3a_1$ (84%)<br>**253** (0.05)<br>$3t_2 \rightarrow 2a_1$ (84%)<br>**290** (0.03)<br>$4t_2 \rightarrow 2a_1$ (89%) | 300 (broad) | **282** (0.08)<br>5t → 3a (57%)<br>5t → 9t (34%)<br>**303** (0.02)<br>5t → 2a (53%)<br>5t → 8t (41%)<br>**313** (0.07)<br>5t → 2e (42%)<br>5t → 6t (26%)<br>5t → 7t (25%) | 260 (broad) | **236** (0.02)<br>7e → 9e (37%)<br>**237** (0.01)<br>6a → 9a (81%)<br>**262** (0.03)<br>6a → 7a (62%)<br>6a → 8a (28%)<br>**266** (0.03)<br>7e → 7a (83%) | 300 (broad) | **247** (0.01)<br>4e → $4a_2$ (37%)<br>$2a_2 \rightarrow 6e$ (37%)<br>**248** (0.02)<br>$2a_2 \rightarrow 6e$ (30%)<br>$2a_2 \rightarrow 7e$ (14%)<br>$2b_2 \rightarrow 8e$ (11%)<br>**284** (0.01)<br>$2b_2 \rightarrow 7e$ (40%)<br>4e → $3b_1$ (21%)<br>$2b_2 \rightarrow 6e$ (14%)<br>**324** (0.01)<br>4e → $3a_1$ (53%)<br>$2b_2 \rightarrow 5e$ (29%)<br>4e → $3b_2$ (13%)<br>**326** (0.01)<br>$2b_2 \rightarrow 3a_1$ (47%)<br>4e → 5e (24%) |
| emission $\lambda$ nm | **533** ($T_1 \rightarrow S_0$) | 405 (8 K)<br>545 (290 K) | **475** ($T_2 \rightarrow S_0$)<br>**517** ($T_1 \rightarrow S_0$) | **523** (290 K) | **574** ($T_1 \rightarrow S_0$) | **412** (8 K)<br>**560** (290 K) | **464** ($T_2 \rightarrow S_0$)<br>**505** ($T_1 \rightarrow S_0$) |

[a] Values in brackets are the oscillator strengths associated with the absorption wavelengths. Only the major contributions to these transitions are indicated with their corresponding weights in %.

L = $NH_3$, $PH_3$) clusters[36] and $[Cu_4I_4py_4]$.[9] This orbital is also present in $[Cu_4I_4(PH_3)_4]$ and in clusters **2** and **3** (Supporting Information, Figure S7). It is the LUMO of $[Cu_4I_4(PH_3)_4]$ and **2**, whereas it lies just above the $\pi^*$(phenyl) combinations in **3** as for **1**. Thus, there are 24 and 16 $\pi^*$(phenyl) combinations for **1** and **3**, respectively, which constitute the lowest unoccupied block of orbitals, lying just below the 4s/4p(Cu) bonding level.

Following the approach of De Angelis et al.,[9] the two lowest triplet states of cluster **1** have been calculated. One of them ($T_2$) was obtained by simply promoting an electron into the $\pi^*$(phenyl) LUMO of the $S_0$ state. The other triplet state ($T_1$) corresponds to the promotion of an electron into the $a_1$ LUMO+24 of $S_0$. This state was obtained by running the optimization process with a starting molecular geometry in which the Cu−Cu distances were shortened in such a way that the LUMO+24 (4a) of $S_0$ becomes the LUMO of this starting geometry and thus is singly occupied in the triplet state. The relative energies of the computed triplet states with respect to the $S_0$ ground state are given in Table 2. The energy difference of $T_1$ and $T_2$ is only 0.09 eV, but they exhibit significantly different structural features (see Table 2). $T_1$ shows large geometrical variations with respect to the ground state. The Cu−I and I−I distances increase whereas the Cu−Cu distances decrease importantly, because of the occupation of the metal−metal bonding orbital of 4s/4p(Cu) type (4a; LUMO+24 in $S_0$). The occupation of this orbital by an electron in $T_1$ results in its stabilization associated with substantial Cu−Cu shortening. The structural features of the other triplet state ($T_2$) do not differ much from that of $S_0$. Indeed, it corresponds to the promotion of an electron from a more or less nonbonding HOMO into a $\pi^*$(phenyl) combination, thus leaving the $[Cu_4I_4]$ core barely affected. In contrast with the $T_1$ state, the MO diagrams of $T_2$ and $S_0$ are quite similar. Similar calculations on cluster **3** yielded similar $T_2$ and $T_1$ states, with single occupation of a $\pi^*$(phenyl) combination in the former and of the Cu−Cu bonding $a_1$ orbital in the latter. Note that in that case, $T_2$ lies 0.42 eV *below* $T_1$. On the other hand a unique low-lying triplet state ($T_1$) was found in the cases of $[Cu_4I_4(PH_3)_4]$ and **2**, which corresponds to the single occupation of their Cu−Cu bonding $a_1$ LUMO and which consequently exhibits Cu−Cu distances significantly shorter than in the $S_0$ state (Table 2).

**Computed versus Experimental UV−visible Absorption and Emissions.** The absorption spectra of clusters **1**−**3** recorded in dichloromethane are shown in Figure 9. The electronic transitions of lowest energy have been computed by the means of TDDFT (see Computational Details). The computed transitions are also reported in Figure 9, their height being proportional to their oscillator strength. The corresponding calculated and experimental data are given in Table 3. The spectrum of cluster **1** exhibits a broad band centered at 300 nm which is in fair agreement with the calculated transitions (282, 303, and 313 nm). All these transitions correspond to an electron promotion from the triply degenerated 5t HOMO to one of the lowest $\pi^*$(phenyl) combination set (2e to 9t). Because of the composition of these orbitals, these transitions can be described as resulting from a mixture of $^1$XLCT and $^1$MLCT charge transfer transitions. Note that the LUMO+24 (4a) is not involved in these low energy transitions. The calculated spectrum of **3** exhibits the same features as that of **1**, with low-energy transitions at 247, 248, 284, 324, and 326 nm which are associated with the


dx.doi.org/10.1021/ic201128a |*Inorg. Chem.* 2011, 50, 10682–10692

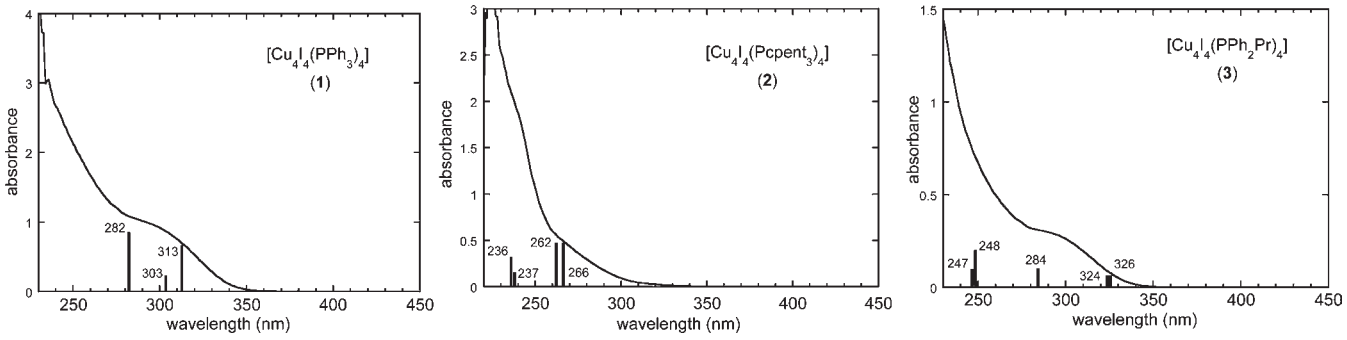


**Figure 9.** Experimental absorption spectra of **1**−**3** in dicloromethane and calculated transitions with bar heights proportional to the oscillator strengths.

two highest occupied t levels and the lowest vacant $\pi^*$(phenyl) combinations (mixed $^1$XLCT/$^1$MLCT charge transfer transitions). On the other hand, the first computed transitions of $[Cu_4I_4(PH_3)_4]$ and **2** correspond to the promotion of an electron from one of the highest occupied mixed Cu/I levels on some of the lowest vacant levels which are all of large metal character, thus corresponding to a mixed XMCT and Cu d → s, p transition.

The emissions of the clusters have been calculated as the differences between the energy of each of the optimized $T_1$ and $T_2$ states and that of the singlet state assuming the same (unrelaxed) geometry as that of the considered triplet state. The corresponding computed values are given in Table 3, together with the experimental values for the sake of comparison. The unique value calculated for **2** (574 nm) is in a rather good agreement with the corresponding experimental one (523 nm at 290 K), namely, the LE band. The same transition corresponds to the $T_1 \rightarrow S_0$ emission in **1**. The calculated value (517 nm) can be correlated to the observed LE band at 545 nm. The second emission of **1** corresponds to the $T_2 \rightarrow S_0$ transition with computed value at 475 nm which can be correlated to the observed HE band observed at 405 nm (8 K). A similar assignment can be made for **3** with a computed LE band at 505 nm and a computed HE band at 464 nm to be compared with the respective 560 and 412 nm experimental data.

## DISCUSSION

The luminescence properties observed for the phosphine-based clusters **1** and **3** arise from two emission bands (LE and HE) whose respective intensity vary with the temperature. In accordance with the DFT calculations, the following band assignment can be suggested for the LE and HE emissions observed. The green LE emission corresponds to the transition from the Cu−Cu bonding $a_1$ symmetry orbital, namely, the LUMO+24 and LUMO+16 for **1** and **3**, respectively, which lie just above the block of MOs based on the $\pi^*$ orbitals of the phenyl groups. According to the nature of the molecular orbitals involved in this transition, this band is assigned to a combination of an iodide-to-copper charge transfer transition (XMCT) and of a copper-centered 3d → 4s, 4p transition. This emission is called "Cluster Centered" ($^3$CC) as it is mainly based on the $[Cu_4I_4]$ cluster core and is essentially independent of the nature of the ligand. The low temperature blue emission (HE) corresponds to a transition from the LUMOs which are combinations of the $\pi^*$ orbitals of the phenyl groups to the HOMO so to an iodide/copper-to-ligand charge-transfer transition with mixed $^3$XLCT/$^3$MLCT character. The occurrence of the blue band is directly correlated to the presence of $\pi^*$ orbitals of the ligand. This is in accordance with the unsaturated character of the $PPh_3$ and $PPh_2Pr$ ligands in clusters **1** and **3**, respectively. The blue band of clusters **1** ($\lambda_{max}$ = 405 nm) and **3** ($\lambda_{max}$ = 412 nm) appears at similar wavelengths agreeing with the similarity of the ligands involved. Note for $[Cu_4I_4py_4]$ in solid-state, the band at 77 K is reported at 438 nm.[8] The vibronic structure of the blue band observed for cluster **1** must originate from ligand centered vibration modes. The lack of luminescence thermochromism for cluster **2** can be easily attributed to the saturated character of $P(cpent)_3$ ligand which does not display a $\pi^*$ orbital and thus a second emission band. Calculations reported for $[Cu_4I_4py_4]$ are globally in agreement with this band attribution.[9] However, compared to our clusters whose HOMOs are equally composed of iodide and copper orbitals, the HOMO of the pyridine derivative is mainly based on iodine orbitals with smaller contribution of copper atoms. Thus, in contrast with the phosphine clusters, the HE band of $[Cu_4I_4py_4]$ has no mixed character but is $^3$XLCT.

From the TDDFT calculations, the broad absorption band experimentally observed for clusters **1** and **3** corresponds to a mixture of $^1$XLCT and $^1$MLCT charge transfer transitions. This is different for cluster **2** whose absorption band is attributed to a $^1$CC transition. For $[Cu_4I_4py_4]$, the two bands ($^1$XLCT and $^1$CC) have been reported and correlated with the two different excitation spectra exhibited by the HE and LE bands.[9] This is thus different for clusters **1** and **3** with no $^1$CC transition but the single absorption band is in agreement with the similar excitation spectra experimentally observed for the two emission bands of **1** and **3** (Figures 5−7).

The thermochromic luminescence displayed by clusters **1** and **3** derives from the two separate excited states, $^3$CC ($T_1$) and $^3$XLCT/$^3$MLCT ($T_2$) mentioned below, with populations varying with the temperature. At low temperature, only the $^3$XLCT/$^3$MLCT state is populated giving rise to the blue emission observed (HE). By increasing the temperature, the CC state is progressively populated at the expense of the latter thanks to increasing vibration energies. Figure 10 illustrates a simplified photophysical model that we suggest for the phosphine-based clusters according to the above data and previous studies on pyridine-based clusters.[9,39] The emission lifetime study is in accordance with this model. The values determined for $[Cu_4I_4(PPh_3)_4]$ (**1**) ($\tau^{LE}_{290K}$ = 4.3 $\mu$s, $\tau^{HE}_{77K}$ = 14.2 $\mu$s, $\tau1^{LE}_{77K}$ = 6.4 $\mu$s, and $\tau2^{LE}_{77K}$ = 15.4 $\mu$s) are in the same range compared to those reported for $[Cu_4I_4(py)_4]$ in solid state ($\tau^{LE}_{298K}$ = 11.1 $\mu$s, $\tau^{HE}_{77K}$ = 23.2 $\mu$s, $\tau^{LE}_{77K}$ = 25.5 $\mu$s).[4] The specific feature of the LE band lifetime observed for **1** at low temperature with a rising time followed by an exponential decay


dx.doi.org/10.1021/ic201128a |Inorg. Chem. 2011, 50, 10682–10692

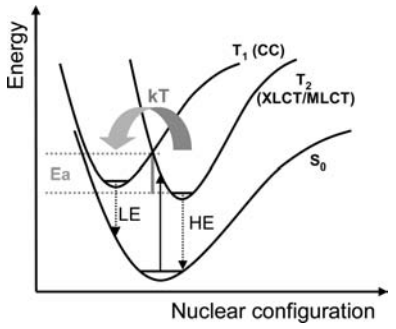


**Figure 10.** Simplified energy level diagram of clusters studied: $[Cu_4I_4L_4]$ L = phosphine.

is totally in agreement with the thermal population of the $^3$CC excited state from the ($^3$XLCT/$^3$MLCT) state. The fact that only a single exponential decay is observed for the LE band at 290 K can be explained by a much faster thermal transfer that can not be observed at this temperature. At 77 K, both LE and HE bands present similar lifetimes that is in accordance with the competition between these two transitions.

The much larger Stokes shift between excitation and emission maxima observed for the LE band compared to the HE one, is attributed to larger distortion of the CC state relative to the ground state, in accordance with the calculations. Actually, upon excitation, strong geometrical relaxation of the $^3$CC state occurs because of electron redistribution associated with distortions of the $[Cu_4I_4]$ core. This distortion is accompanied with an increase of Cu−I and an important decrease of Cu−Cu distances with respect to the ground state, in agreement with the nature of the states involved (see DFT calculations). The electron emission transition is indeed from the LE excited state which has Cu−I antibonding and Cu−Cu bonding character to the nonbonding HOMO. As represented in Figure 10, rearrangement of the HE state is more limited with almost unaffected geometry. A similar behavior has been reported for the pyridine cluster.[9]

In a previous study, ab initio calculations at the Hartree−Fock level have been investigated and have demonstrated a relationship between the Cu−Cu distances and the energy of distortion in the LE excited state relative to the ground state for two different clusters; $[Cu_4I_4(py)_4]$ and $[Cu_4X_4(dpmp)_4]$ (dpmp = 2-DiPhenylMethylPyridine).[40] The reduced Cu−Cu interaction in $[Cu_4X_4(dpmp)_4]$ ($d_{Cu-Cu}$ = 2.90 Å) has been reported to lead to less distortion compared to $[Cu_4I_4(py)_4]$ ($d_{Cu-Cu}$ = 2.69 Å) and thus to better communication between the XLCT and the CC states. Accordingly, the LE band of $[Cu_4X_4(dpmp)_4]$ has a very low intensity because of non radiative deactivation of the CC state to the XLCT one ($E_a$ = 1000 cm$^{-1}$), and this study suggested that only compounds with Cu−Cu distances shorter than 2.8−2.9 Å exhibit emissive CC states (van der Waals radius of Cu(I) = 1.4 Å).[4,40] This is clearly not the case for clusters **2**−**3** which display highly intense LE emission with average Cu−Cu bond length even over 3 Å (2.901(1), 3.276(1), and 3.14(8) Å for **1**, **2**, and **3**, respectively). Thus, despite longer Cu−Cu distances, **1**−**3** clusters are comparable to $[Cu_4I_4(py)_4]$ which displays two highly emissive states. So, it seems that phosphine-based clusters represent a different case with luminescence behavior closer to $[Cu_4I_4(py)_4]$ than to $[Cu_4X_4(dpmp)_4]$ clusters despite long Cu−Cu contacts. As already mentioned, in contrast to $[Cu_4I_4(py)_4]$ which displays different excitation spectra for the LE and HE bands, those recorded at 100 K for **3** and at 80 K for **1** (Figure 5a and 7a) are similar. This means that theses emissions originate from one common excitation state which then deactivates on the XLCT emission state and afterward, when the temperature increases, on the CC state. This suggests that these two emissive states are highly coupled in the phosphine based clusters; that is not the case for the pyridine derivative.

Upon lowering the temperature, the LE emission band of cluster **1** is red-shifted (Figure 5b). Recently, the position of the LE band has been correlated to the Cu−Cu distances in the $[Cu_4I_4]$ cluster core.[41,26] Indeed, from the DFT calculations, the Cu−Cu interactions in the excited state ($T_1$) are of bonding character. As the temperature decreases, the Cu−Cu distances become shorter, the bonding character increases, the energy level is lowered, and thus the LE emission band shifts to longer wavelength: from 547 nm at 290 K to 570 nm at 120 K for **1**. In Figure 10, this corresponds to a left shift of the $T_1$ curve relative to the ground state one. This phenomenon has been also reported for $[Cu_4I_4py_4]$ in the solid state with values of 580 nm at 298 K and 619 nm at 77 K.[8,42,43] This LE emission band shift observed for cluster **1** but not for **2** and **3** can be related to the Cu−Cu distances found in the three clusters (Table 2). As already mentioned, cluster **1** has Cu−Cu distances much shorter (2.901(1) Å) compared to the two other ones (3.276(1) and 3.14(8) Å for **2** and **3**, respectively). These long values imply no or weak Cu−Cu interactions in clusters **2** and **3**, and decreasing the temperature is not enough to induce significant metallic interaction. This explains the absence of variation of the CC excited state energy and LE band shift. Cu−Cu contacts seem to be, in this emission shift phenomenon, an essential parameter. The fact that these distances are longer for clusters **2** and **3** compared to cluster **1** and do not present significant shortening by lowering the temperature may be attributed to steric effect of the ligands to the $[Cu_4I_4]$ cluster core and/or to crystal packing.

For cluster **3**, the absence of band shifting by varying the temperature leads to an isoemissive point in the emission spectra (Figure 7b). In the 60−140 K range, an activation energy value of 483 cm$^{-1}$ has been determined. This value corresponds to the energy barrier to populate the LE emission state from the HE one and is illustrated in Figure 10. For pyridine derivatives, higher values of activation energy have been reported, namely, 1000 cm$^{-1}$ for $[Cu_4Br_4(dpmp)_4]$ (dpmp = 2-DiPhenylMethylPyridine) cluster,[44] and 800 cm$^{-1}$ for $[Cu_4I_4py_4]$.[45] This indicates a lower energy barrier between the two LE and HE states for the phosphine derivatives compared to the pyridine ones. In addition to similar excitation profiles, this also indicates very high coupling of the two emissive states for phosphine based clusters. This leads in this case, to a very controlled luminescence thermochromism and to our knowledge this has never been observed for copper iodide $[Cu_4I_4]$ clusters. It is interesting to note that when this cluster is grafted to a silica matrix, luminescence thermochromism is controlled in a much larger temperature range.[12] This can be explained by less constraint and higher thermal vibrations in the pure cluster materials.

## CONCLUSION

This study reports on the synthesis, structural characterization, DFT/TDDFT calculations, and temperature dependence of photoluminescence measurements of copper iodide clusters coordinated by three different phosphine ligands. Photophysical studies of these phosphine-based clusters and especially correlation

between experimental (structural and optical) and theoretical data and comparison with previous works on pyridine-based clusters, provide new insights into a complicated photophysical system.

Under UV excitation, two intense emissions are observed for the clusters studied with a bright green-yellow luminescence at room temperature which becomes blue at low temperature. The DFT calculations are in agreement with the following band assignment. The LE band originates from a $[Cu_4I_4]$ cluster centered excited state (CC) whereas the HE one involves a mixed charge-transfer (MLCT/XLCT) excited state which differs from $[Cu_4I_4py_4]$. As the $\pi^*$ orbitals of the ligands are involved in this XLCT band, the emission at low temperature is only observed for clusters incorporating $\pi$-unsaturated ligands such as clusters **1** and **3**. The thermochromic luminescence exhibited by these clusters derives from the thermal equilibrium between two separate excited states (MLCT/XLCT and CC). In contrast with the pyridine derivatives, same excitation states and low activation energy for these clusters reflect high coupling of the two emissive states.

The effect of the Cu−Cu interactions on the emission properties of these clusters is not so obvious. Particularly, our results disagree with previous studies suggesting that only compounds with Cu−Cu distances shorter than 2.8−2.9 Å exhibit emissive CC states. For the LE band emission observation, the Cu−Cu contacts do not seem to be an essential parameter. However, for the red shifting of the LE band, only observed for cluster **1** when the temperature decreases, this distance must be apparently close to the 2.8 Å van der Waals contact value of Cu(I) to have significant influence on the CC excited state energy. An interesting feature is displayed by cluster **3** with long Cu−Cu contacts for which no band shifting is observed in temperature. This leads to a perfectly controlled thermochromic luminescence which has been to our knowledge unknown in this family of copper iodide clusters.

To conclude, rich photoluminescence properties are exhibited by the phosphine-based copper iodide clusters. Compared to pyridine derivatives, they are more stable and thus particularly interesting for the synthesis of original emissive materials. Moreover, they have the advantage of the low cost and relatively easy synthesis. Work is in progress in our laboratory to prepare new cluster-based materials by incorporation of phosphine derivatives into amorphous polymeric matrixes.

## ■ ASSOCIATED CONTENT

**Supporting Information.** The X-ray crystallographic file (CIF), DFT and other characterization data. This material is available free of charge via the Internet at http://pubs.acs.org.

## ■ AUTHOR INFORMATION

### Corresponding Author

*Fax: (+33) (0)1 69 33 47 99. Phone: (+33) (0)1 69 33 46 51. E-mail: sandrine.perruchas@polytechnique.edu (S.P.), jean-pierre.boilot@polytechnique.fr (J.-P.B.).

## ■ ACKNOWLEDGMENT

The authors thank the CNRS for financial help and for the postdoctoral fellowship of C.T. J.-Y.S. thanks the IUF for its support.

## ■ REFERENCES

(1) Jüstel, T.; Nikol, H.; Ronda, C. *Angew. Chem., Int. Ed.* **1998**, *37*, 3084.
(2) Pénard, A.-L.; Gacoin, T.; Boilot, J.-P. *Acc. Chem. Res.* **2007**, *40*, 895.
(3) Barbieri, A.; Accorsi, G.; Armaroli, N. *Chem. Commun.* **2008**, 2185.
(4) Ford, P. C.; Cariati, E.; Bourasssa, J. *Chem. Rev.* **1999**, *99*, 3625, and references therein.
(5) Yam, V. W.-W.; Lo, K. K.-W. *Chem. Soc. Rev.* **1999**, *28*, 323.
(6) Vitale, M.; Ford, P. C. *Coord. Chem. Rev.* **2001**, *219*, 3.
(7) Hardt, H. D.; Pierre, A. *Z. Anorg. Allg. Chem.* **1973**, *402*, 107.
(8) Kyle, K. R.; Ryu, C. K.; DiBenedetto, J. A.; Ford, P. C. *J. Am. Chem. Soc.* **1991**, *113*, 2954.
(9) De Angelis, F.; Fantacci, S.; Sgamellotti, A.; Cariati, E.; Ugo, R.; Ford, P. C. *Inorg. Chem.* **2006**, *45*, 10576.
(10) Kim, T. H.; Lee, K. Y.; Shin, Y. W.; Moon, S.-T.; Park, K.-M.; Kim, J. S.; Kang, Y.; Lee, S. S.; Kim, J. *Inorg. Chem. Commun.* **2005**, *8*, 27.
(11) Knorr, M.; Guyon, F.; Khatyr, A.; Daschlein, C.; Strohmann, C.; Aly, S. M.; Abd-El-Aziz, A. S.; Fortin, D.; Harvey, P. D. *Dalton Trans.* **2009**, 948.
(12) Tard, C.; Perruchas, S.; Maron, S.; Le Goff, X. F.; Guillen, F.; Garcia, A.; Vigneron, J.; Etcheberry, A.; Gacoin, T.; Boilot, J.-P. *Chem. Mater.* **2008**, *20*, 7010.
(13) Churchill, M. R.; Kalra, K. L. *Inorg. Chem.* **1974**, *13*, 1899.
(14) Arkhireeva, T. M.; Bulychev, B. M.; Sizov, A. I.; Sokolova, T. A.; Belsky, V. K.; Soloveichik, G. L. *Inorg. Chim. Acta* **1990**, *169*, 109.
(15) Churchill, M. R.; Rotella, F. J. *Inorg. Chem.* **1977**, *16*, 3267.
(16) Dyason, J. C.; Healy, P. C.; Engelhardt, L. M.; Pakawatchai, C.; Patrick, V. A.; Raston, C. L.; White, A. H. *J. Chem. Soc., Dalton Trans.* **1985**, 831.
(17) Lai, D. C.; Zink, J. I. *Inorg. Chem.* **1993**, *32*, 2594.
(18) (a) Stepnicka, P.; Gyepes, R.; Podlaha, J. *Collect. Czech. Chem. Commun.* **1998**, *63*, 64. (b) Stepnicka, P.; Cisarova, I. *Collect. Czech. Chem. Commun.* **2006**, *71*, 215.
(19) Medina, I.; Mague, J. T.; Fink, M. J. *Acta Crystallogr., Sect. E* **2005**, *61*, m1550.
(20) Herberhold, M.; Akkus, N.; Milius, W. *Z. Anorg. Allg. Chem.* **2003**, *629*, 2458.
(21) Lobana, T. S.; Kumar, R.; Sharma, R.; Nishioka, T.; Castineiras, A. *J. Coord. Chem.* **2005**, *58*, 849.
(22) Seddigi, Z. S.; Hossain, G. M. G.; Banu, A. *Acta Crystallogr., Sect. E* **2007**, *63*, m756.
(23) Li, Y.; Yung, K.-F.; Chan, H.-S.; Wong, W.-T. *Inorg. Chem. Commun.* **2003**, *6*, 1451.
(24) Perruchas, S.; Le Goff, X. F.; Maron, S.; Maurin, I.; Guillen, F.; Garcia, A.; Gacoin, T.; Boilot, J.-P. *J. Am. Chem. Soc.* **2010**, *132*, 10967.
(25) Attar, S.; Bowmaker, G. A.; Alcock, N. W.; Frye, J. S.; Bearden, W. H.; Nelson, J. H. *Inorg. Chem.* **1991**, *30*, 4743.
(26) Kitagawa, H.; Ozawa, Y.; Toriumi, K. *Chem. Commun.* **2010**, *46*, 6302.
(27) Bril, A. *Philips Res. Rep.* **1964**, *306*, 19296.
(28) Altomare, A.; Burla, M. C.; Camalli, M.; Cascarano, G.; Giacovazzo, C.; Guagliardi, A.; Moliterni, A. G. G.; Polidori, G.; Spagna, R. *SIR97, an integrated package of computer programs for the solution and refinement of crystal structures using single crystal data*; CNR-IC: Bari, Italy.
(29) Sheldrick, G. M. *SHELXL-97*, Universität Göttingen, Göttingen, Germany, 1997.
(30) Frisch, M. J.; Trucks, G. W.; Schlegel, H. B.; Scuseria, G. E.; Robb, M. A.; Cheeseman, J. R.; Montgomery, J. A. Jr.; Vreven, T.; Kudin, K. N.; Burant, J. C.; Millam, J. M.; Iyengar, S. S.; Tomasi, J.; Barone, V.; Mennucci, B.; Cossi, M.; Scalmani, G.; Rega, N.; Petersson, G. A.; Nakatsuji, H.; Hada, M.; Ehara, M.; Toyota, K.; Fukuda, R.; Hasegawa, J.; Ishida, M.; Nakajima, T.; Honda, Y.; Kitao, O.; Nakai, H.; Klene, M.; Li, X.; Knox, J. E.; Hratchian, H. P.; Cross, J. B.; Bakken, V.; Adamo, C.; Jaramillo, J.; Gomperts, R.; Stratmann, E.; Yazyev, O.; Austin, A. J.; Cammi, R.; Pomelli, C.; Ochterski, J. W.; Ayala, P. Y.; Morokuma, K.; Voth, G. A.; Salvador, P.; Dannenberg, J. J.; Zakrzewski, V. G.; Dapprich, S.; Daniels, A. D.; Strain, M. C.; Farkas, O.; Malick, D. K.; Rabuck, A. D.;

Raghavachari, K.; Foresman, J. B.; Ortiz, J. V.; Cui, Q.; Baboul, A. G.; Clifford, S.; Cioslowski, J.; Stefanov, B. B.; Liu, G.; Liashenko, A.; Piskorz, P.; Komaromi, I.; Martin, R. L.; Fox, D. J.; Keith, T.; Al-Laham, M. A.; Peng, C. Y.; Nanayakkara, A.; Challacombe, M.; Gill, P. M. W.; Johnson, B.; Chen, W.; Wong, M. W.; Gonzalez, C.; Pople, J. A. *Gaussian 03*, revision E.01; Gaussian, Inc.: Wallingford, CT, 2004; http://www.gaussian.com.

(31) (a) Perdew, J. P.; Ernzerhof, M.; Burke, K. *J. Chem. Phys.* **1996**, *105*, 9982. (b) Perdew, J. P.; Burke, K.; Ernzerhof, M. *Phys. Rev. Lett.* **1996**, *77*, 3865. (c) Perdew, J. P.; Burke, K.; Ernzerhof, M. *Phys. Rev. Lett.* **1997**, *78*, 1396.

(32) (a) Dunning, T. H., Jr.; Hay, P. J. *Methods of Electronic Structure Theory*; Schaefer, H. F., Ed.; Plenum Press: New York, 1977. (b) Hay, P. J.; Wadt, W. R. *J. Chem. Phys.* **1985**, *82*, 270. (c) Hay, P. J.; Wadt, W. R. *J. Chem. Phys.* **1985**, *82*, 284. (d) Hay, P. J.; Wadt, W. R. *J. Chem. Phys.* **1985**, *82*, 299.

(33) Gorelsky, S. I. *AOMix program*; http://www.sg-chem.net.

(34) Burke, K.; Gross, E. K. U. A guided tour of time-dependent density functional theory. In *Density Functionals: Theory and Applications, Lecture Notes in Physics*; Joubert, D., Ed.; Springer: New York, 1998; Vol. 500.

(35) Flukiger, P.; Luthi, H. P.; Portmann, S.; Weber, J. *MOLEKEL*, 4.3; Swiss Center for Scientific Computing: Manno, Switzerland, 2000; http://www.cscs.ch/.

(36) Vega, A.; Saillard, J.-Y. *Inorg. Chem.* **2004**, *43*, 4012.

(37) Raston, C. L.; White, A. H. *J. Chem. Soc., Dalton Trans.* **1976**, 2153.

(38) Bondi, A. *J. Phys. Chem.* **1964**, *68*, 441.

(39) Vitale, M.; Palke, W. E.; Ford, P. C. *J. Phys. Chem.* **1992**, *96*, 8329.

(40) Vitale, M.; Ryu, C. K.; Palke, W. E.; Ford, P. C. *Inorg. Chem.* **1994**, *33*, 561.

(41) Kim, T. H.; Shin, Y. W.; Jung, J. H.; Kim, J. S.; Kim, J. *Angew. Chem., Int. Ed.* **2008**, *47*, 685.

(42) Vogler, A.; Kunkely, H. *J. Am. Chem. Soc.* **1986**, *108*, 7211.

(43) Tran, D.; Bourassa, J. L.; Ford., P. C. *Inorg. Chem.* **1997**, *36*, 439.

(44) Ryu, C. K.; Vitale, M.; Ford, P. C. *Inorg. Chem.* **1993**, *32*, 869.

(45) Radjaipour, M.; Oelkrug, D. *Ber. Bunsen-Ges. Phys. Chem.* **1978**, *82*, 159.